RELIABILITY OF TERRESTRIAL IMAGE GEO-REFERENCING USING GPS AND MEMS INERTIAL MEASUREMENT UNIT

J. Kolecki [a, *], P. Kuras [a]

[a] Faculty of Mining Surveying and Environmental Engineering, AGH University of Science and Technology, Poland
(kolecki, kuras)@agh.edu.pl

KEY WORDS: Direct geo-referencing, Mobile mapping, IMU, GPS, Bundle adjustment, Reliability estimation

ABSTRACT:

Recently the technology of terrestrial mobile mapping systems has developed rapidly. However such systems are large–sized, heavy and expensive mostly due to high costs of inertial sensors. To overcome above problems, low-cost, small navigation sensors like MEMS IMUs can be used instead to provide geo-referencing of acquired images. The observation integration methodology in such systems is slightly different. In contrast to the commercial systems, where both real-time Kalman filtering and the post-mission smoothing algorithms are used, the integration of observations in low-cost system is based mostly on the integrated bundle adjustment. In this paper we will look at some network quality measures in the context of direct geo–referencing and examine some network configurations that may be realized using low–cost MMSs. Firstly the redundancy and reliability measures will be introduced. Then the MMS prototype used in the experiments will be characterized. Afterwards the testing strategy and test fields will be described. Finally the results and conclusions will be given. The results show that the reliability of EO measurements is better in nonlinear network configurations. In such image configurations the angle errors, which are usually high due to the low accuracy of inertial and magnetic sensors, would not affect the finally estimated EO parameters and object point coordinates. The results show that the proper design of the photogrammetric network, in which the GPS and photogrammetric observations play most important role, could increase the reliability and accuracy of image geo-referencing. The achieved accuracies are satisfactory for all tested networks.

1. INTRODUCTION

1.1 Overview

The mobile mapping technology involves combining images or measurements taken by various sensors. The integration usually takes place in two steps. In the first one, the measurements carried out by navigation and positioning sensors, like IMU and GPS, are combined to provide most accurate geo–referencing of images or laser scans. The integration methodology typically involves Kalman filtering and post–mission smoothing to provide the optimal trajectory estimation. The second step involves integration of photogrammetric observations to provide better adjustment of acquired images. This is usually achieved within the bundle adjustment procedure, in which previously estimated exterior orientation (EO) parameters can be treated also as observed values.

Such strategy is common in aerial photogrammetry supported by GPS/INS integrated systems. Initial values of the EO parameters are not accurate enough to satisfy demands of most photogrammetric products. As a consequence the bundle adjustment is the natural way to improve them. On the other hand, in commercial terrestrial mobile mapping systems, images are used usually to support laser scans, and their EO can be estimated quite well, so often no further integration involving bundle adjustment is required. As commercial terrestrial MMSs are very expensive, large–sized and heavy, the researches on low–cost systems are conducted. Such systems often do not use inertial measurements or use MEMS or some inexpensive tactical grade IMUs. However in this case low–cost means also lower accuracy, and the further improvement of image EO parameters, often involving bundle adjustment, has to be carried out. The achieved results depends not only on accuracy of GPS and inertial measurements, but also on the geometry of the image network or sequence.

1.2 Related work

Recently few low-cost MMSs designed to perform road and highway measurements have been developed. Piras (Piras *et al*, 2008) uses the L1 GPS set, gyroscope and odometer to capture geo–referenced stereo images, that are used in road surveys. However no further adjustment of images is subsequently done. Madeira (Madeira *et al*, 2008) uses more accurate positioning devices: L1+L1 GPS set with two antennas and tactical grade IMU. The GPS and inertial measurements are integrated using Kalman filter to determine image EO parameters. As Piras, Madeira does not perform the bundle adjustment of acquired images. Da Silva (da Silva *et al*, 2003) investigated a van MMS comprised of two cameras and a single-frequency GPS set. The azimuth of camera axes is determined from coordinates of two consecutive exposure stations. Other angular EO elements are initially assumed to equal zero. The coordinates of projection centres (PCs) are determined directly from GPS coordinates. Da Silva performs the bundle adjustment of stereo–pair sequence to improve the accuracy of initially determined EO parameters. The achieved accuracies satisfie the demands of road cadastral surveys.

Besides van MMSs, also portable, hand–held mapping or navigation systems have been developed. Haala and Böhm (2003) present a kind of pedestrian system designed for positioning in urban environments. They integrate

* Corresponding author

measurements from the digital compass, inclinometer and GPS with 3D building data base in order to identify buildings captured by camera. Ellum and El–Sheimy (2001) developed a backpack MMS. They use L1+L2 GPS set to measure coordinates of PCs and digital compass with inclinometer to determine angular EO parameters of acquired images. Subsequently they perform the bundle adjustment, achieving a considerable improvement of accuracy. The relative accuracies reported by Ellum and El–Sheimy were in many cases much better than 10 cm. Ellum and El–Sheimy also include the distance observation in the bundle adjustment, achieving further accuracy improvement. The Ellum's system prototype was subsequently improved by Coppa (Coppa et al, 2007) who used higher resolution SLR camera instead the compact one. Reported accuracies, after the bundle adjustment, were similar to those achieved by Ellum and El–Sheimy (2001).

Bartelsen and Mayer (2010) show that even a simple GPS camera (RICOH Caplio 500SE) can be regarded as a complete image geo–referencing device. Although no angular EO parameters can be measured, they can be subsequently determined in the two–stage adjustment process. Firstly the image network is adjusted in the local coordinate system using automatically measured tie points. Then the adjusted network is transformed to the global coordinate system utilizing coordinates recorded by GPS during the image acquisition. In both stages the RANSAC procedure is applied to detect gross errors. This enables the whole process to run fully automatically. However due to considerable errors of recorded coordinates, the final geo–referencing and mapping accuracy must be considerably lower than those reported by Ellum and El–Sheimy or by Coppa.

Ellum and El–Sheimy (2005) propose also a deeper integration of photogrammetric and GPS observations. While solving the aerial triangulation, they adjust together with collinearity equations also a code range, double–differenced code range and double–differenced carrier phase observation equations. However such integration strategy has not given better accuracies than those achieved applying a traditional bundle adjustment functional model.

1.3 Reliability

The bundle adjustment allows to find estimators of parameters which are necessary in photogrammetric modeling, namely the image EO elements. In parametric least square adjustment, each parameter is estimated using equations of observed values i.e. observation equations. Observations are the functions of the estimated parameters, and their least square estimates are also found in the adjustment procedure. In the typical geo–referenced image network (like in aerial triangulation) usually two kinds of observation equations appear: the collinearity equations and the observation equations of EO elements. The ground control point coordinates can also be treated as observed values or even as constants, but the concept of direct geo–referencing aim to fully eliminate control points from the photogrammetric workflow.

The amount of each observation, used in the parameter estimation process is different. For each observation, the redundancy factor can be calculated to measure the percentage of observation which was used in the estimation procedure. The redundancy vector is given by the equation (Kraus 1997; Luhmann, 2006):

$$r = diag\left(\hat{Q}_V P\right) \tag{1}$$

where: $\hat{Q}_V$ is the correction cofactor matrix,
P is the weight matrix.

High redundancy means that low percentage of observation was utilized in the parameter estimation. Such observation is highly redundant, but it can be controlled by other observations, so accidental gross errors associated with it can be detected. When the redundancy is low, gross errors can easily influence the values of estimated parameters. For gross error detection the standardized correction test can be applied. The standard deviations of corrections can be calculated as square roots of the correction covariance matrix diagonal elements. This matrix is given by the equation:

$$\hat{C}_V = \hat{\sigma}_0^2 \hat{Q}_V \tag{2}$$

where: $\hat{Q}_V$ is the correction cofactor matrix,
$\hat{\sigma}_0^2$ is the estimator of the variance factor.

The standardized correction of the individual i–th observation is given by:

$$\bar{v}_i = \frac{v_i}{\hat{\sigma}_{v_i}} \tag{3}$$

where: v_i is the correction,
$\hat{\sigma}_{v_i}$ is the standard deviation of i–th correction.

The standardized correction have the $N(0,1)$ distribution, so every correction with value above 2.56 is assumed be gross with probability of 99%. Observations are unequally sensitive to the standardized correction test. The minimal gross error of certain observation which allow its detection is defined as the inner reliability. The inner reliability (IR) of the i–th observation is given by the formula (Kraus, 1997; Luhmann 2006):

$$IR_i = \frac{\delta}{\sqrt{r_i}} \sigma_{l_i} \tag{4}$$

where: δ is the non–centrality parameter (Kraus, 1997),
r_i is the redundancy,
σ_{l_i} is the *a posteriori* observation error.

Inner reliability strongly depends on the redundancy. The non–centrality parameter (δ) is usually set to 4.

The undetected gross error of certain observation affects the values of estimated parameters. Due to such gross error the value of some parameters can change considerably, and the

values of others may change slightly. The value of potential parameter bias caused by observation gross error is called outer reliability. For *i*–th observation the outer reliability vector can be calculated according to following formula:

$$OR_i = \hat{Q}_X A^T P \begin{bmatrix} 0_{i-1\times 1} \\ IR_i \\ 0_{n-1\times 1} \end{bmatrix} \quad (5)$$

where: $\hat{Q}_X$ is the parameter cofactor matrix,
A is the partial derivative matrix,
P is the weight matrix,
0 is the zero vector (size in the index),
IR_i is the inner reliability,
n is the number of observation.

The outer reliability of *i*–th observation with respect to *j*–th parameter (OR_{ij}) corresponds to *j*–th element in the OR_i vector. Outer reliability should be compared to the estimated parameter error to find the potential weakness in photogrammetric network, i.e. the standardized outer reliability should be estimated (similarly to standardized correction):

$$\overline{OR}_{ij} = \frac{OR_{ij}}{\hat{\sigma}_{X_j}} \quad (6)$$

where: OR_{ij} is the outer reliability,
$\hat{\sigma}_{X_j}$ is the estimated parameter error.

The $\overline{OR}_{ij}$ value is the measure of influence the observation has on the parameter. According to Kraus (1997), it should not exceed 3.

The redundancy, inner reliability and outer reliability vector of certain observation depend mostly on:
- geometry of image network,
- weights of observed values.

2. LOW-COST MMS PROTOTYPE

The MMS prototype used in experiments consists of Nikon D80 SLR camera (3872 × 2592 pixels), Leica 1200 set, and low–cost Xsens MTi IMU. The Nikon D80 camera was calibrated with Nikon Nikkor 20 mm f/2.8D lens. Figure 1 shows all devices mounted on the GPS pole.

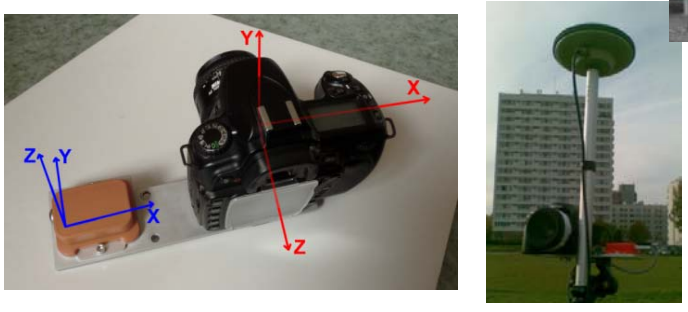

Figure 1. IMU and camera coordinate systems (Kolecki & Kuras, 2011), and the portable MMS prototype

The Leica 1200 set consists of GX1230 GG receiver, AX1202 GG antenna and AX1210T RTK terminal. The real time kinematic (RTK) surveys can be carried out using the corrections determined and distributed by Polish network of reference stations (ASG–EUPOS). The accuracy of the RTK survey is about 1–2 cm for *X* i *Y* coordinates, and about 1.5 factor worse for *Z*.

Xsens MTi IMU consists of inertial sensors (3 gyros and 3 accelerometers) and three magnetometers. All measurements are integrated using the Kalman filter. The calibration of the magnetometers was performed for the construction shown in the figure 1, to compensate for iron effects. In order to obtain the yaw angle estimate in the same coordinate system as the GPS measurements, its value is corrected for magnetic declination and convergence. The Xsens MTi does not provide the estimation of position. However the position can be calculated, but its error is going to grow rapidly. In the designed MMS the MTi unit is used only as AHRS (Attitude and Heading Reference System). According to manufacturer's specifications the *yaw*, *pitch* and *roll* angles are measured with the accuracy of about 1° – 2°, 0.5° and 0.5° respectively. However accuracies achieved for *roll* an *pitch* in previous tests (Kolecki & Kuras, 2011) were found to be much better (about 0.1°).

The boresight calibration of the system was performed on the test–field according to the two step method (Bayoud, 2006). The lever–arm vector was determined in laboratory using tachymeters. The *yaw*, *pitch* and *roll* angles (rotations about Z, Y and X axes) are converted to α, ν and κ angles (Z-X-Z) (Kraus 1997) to obtain better conditioning of the normal equation system during the bundle adjustment (Wrobel & Klemm 1984). For the nearly horizontal images, the *a priori* α error is the same as the *yaw* error. The ν and κ errors correspond to *roll* and *pitch* errors (see coordinate systems in Fig. 1).

3. TESTING

3.1 Test fields

Figures 2 and 3 present objects chosen as our test fields with some check points marked.

Figure 2. Test field #1 – building façade

Figure 3. Test fields #2 – small building

Test field #1 is a building façade, which is appropriate for testing the linear image network with side looking images. Test field #2 is a small building, useful for testing the closed looped image configurations.

3.2 Image networks

Using the constructed MMS prototype 14 images were captured in the test–field #1. Two subsets, each of 6 images, were chosen for further tests (Fig. 4). The first subset was used to construct an image network, with projection centres lying nearly on one straight. The second subset was used to construct a network, consisted of two image rows, with 3 images in each. The pixel diameter for the façade is about 7 mm for closer and about 10 mm for further images. Subsequently 19 images were captured in closed looped configuration in the test field #2. The terrain pixel size was about 1 mm.

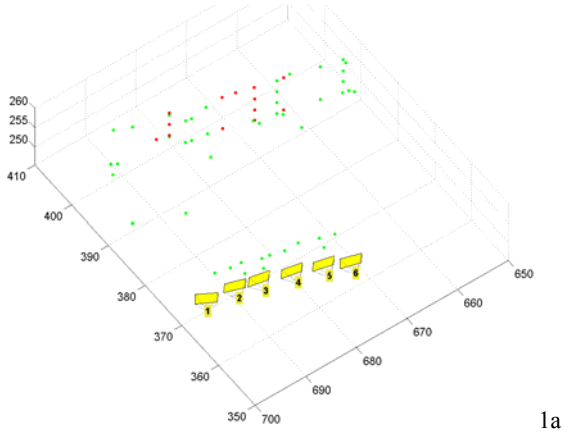

1a

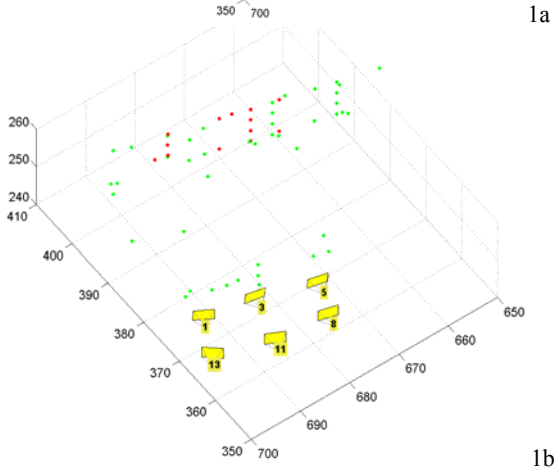

1b

Figure 4. Image networks (no. 1a and 1b) in the test field #1
• – check point, • – tie point

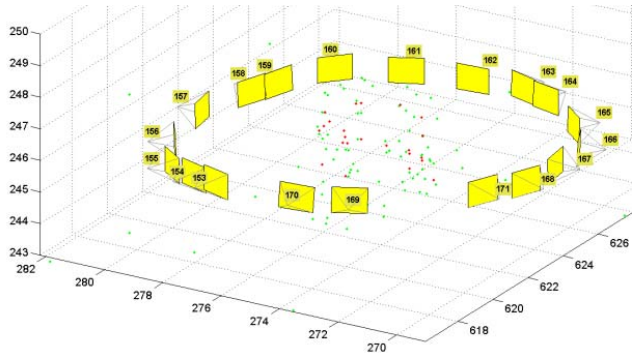

Figure 5. Image network (no. 2) in test field #2
• – check point, • – tie point

For each image *yaw*, *pitch* and *roll* angles were measured 10 times and averaged. After capturing the image, observations for 10 – 20 GPS epochs were recorded.

3.3 Bundle adjustment

The bundle adjustment was calculated for each network according to following assumptions:

- Only observations of image coordinates of tie points, projection centre coordinates and α, ν and κ angles were used in the adjustment.
- The *a priori* error of image coordinates was assumed to be 0.5 pixel.
- The *a priori* errors of projection centre coordinates were assumed to be 20, 20 and 30 mm respectively for X, Y and Z.
- The *a priori* errors of α, ν and κ were chosen according to the manufacturers specification (1-2°, 0.5°, 0.5°).
- Each check point was measured only in 2 images.
- Check point coordinates was not treated as unknowns during the bundle adjustment, but were calculated by photogrammetric intersection, using the estimated EO parameters.

4. RESULTS

4.1 Reliability

Figures 6 and 7 present the standardized outer reliability diagrams for network 1a and 1b. The element in i–th column and j–th row corresponds to the $\overline{OR}_{ij}$ coefficient, given by equation (6). The diagrams (Fig. 6, Fig. 7) are divided into four main parts. In the left upper part the outer reliabilities for observed PC coordinates (columns) with respect to estimated PC coordinates (rows) are given. In the left lower part the reliabilities for observed PC coordinates with respect to estimated angular EO elements are shown. In the right parts the reliabilities of observed angles were placed. 4 main parts are divided further into 3 x 3 boxes, corresponding to individual images.

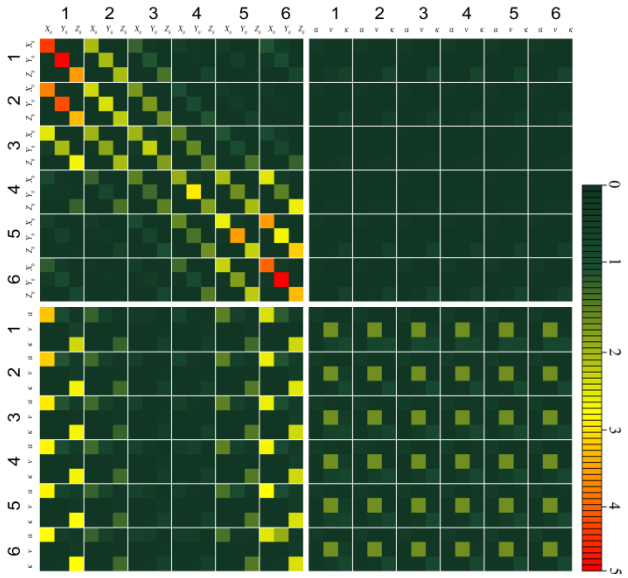

Figure 6. Standardized outer reliability table for observed (columns) and estimated (rows) EO parameters for network 1a

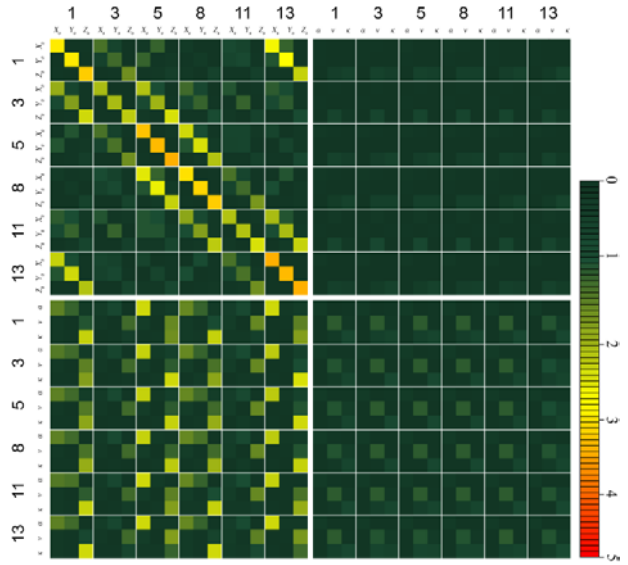

Figure 7. Standardized outer reliability table for observed (columns) and estimated (rows) EO parameters for network 1b

Looking at figures 6 and 7 we see that:

- the critical value of 3 is sometimes exceeded,
- the outer reliability of observed PC coordinates of images 1 and 6 in the 1a network considerably exceeds 3 for estimated PC coordinates of images 1, 2, 5 and 6.
- the observed PC coordinates of images 1 and 6 in the 1a network strongly influence the estimated PC coordinates of all images,
- the observed PC coordinates of image 1 (1a network) influence more the estimated PC coordinates of image 2 than the observation carried out for this image,
- in both networks the estimations of α and κ almost do not depend on the observations of this angles,
- in the network 1a the estimated v angle depends almost equally on observed v angles of all images,
- in the network 1b the estimated v angle depends more on observed Z_0 coordinates, than on observed v angles,
- the observations of α and κ play marginal role in the bundle adjustment,

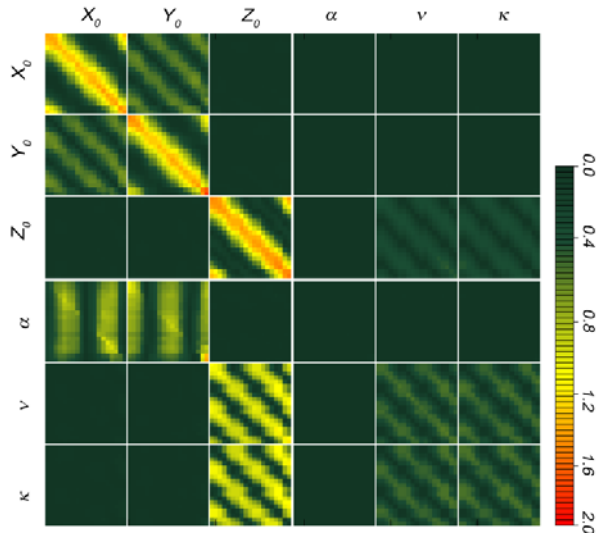

Figure 8. Standardized outer reliability table for observed (columns) and estimated (rows) EO parameters for network 2

In figure 8 the outer reliabilities for network 2 are presented. In this figure the reliability values are grouped according EO parameter names. Image no. 153 (Fig. 5) is first in each group.

Analysing Figure 8 we see that:

- network no. 2 has much better geometry than networks 1a and 1b, possibly due to better image layout and higher image quantity,
- reliabilities do not even approach the value of 3,
- estimated Z_0 coordinates depend almost only on Z_0 observations carried out for considered and neighbour images,
- the estimated X_0 coordinates depend also on observations of Y_0 coordinates carried out for images located 90° left and 90° right from considered image,
- similar rule relate to estimated Y_0 coordinates,
- estimated α angle always depends on observed X_0 and Y_0 coordinates of other image, regardless of proximity to considered image,
- the α/X_0 and α/Y_0 blocks are complementary: the observations of X_0 coordinates carried out for images located in the southern and northern part of the network, and the observation of Y_0 coordinates located in the eastern and western part are mainly used for α angle estimation,
- estimated v and κ angles depend mostly on Z_0 observations,
- estimated v angle depends mostly on Z_0 observations carried out not only for considered and neighbour images, but also for images lying on the opposite side of the loop,
- estimated κ angle depends mostly on Z_0 observations carried out for images located 90° left and 90° right from considered image,
- observations of v and κ angle play marginal role in the bundle adjustment of this network,
- observations of α angle play no role in the solution of the bundle adjustment.

4.2 Accuracy

To assess the accuracy of terrain point measurement, the coordinates of check points were calculated using estimated EO parameters. In the 1a and 1b network, control points were measured in images no. 3 and 5 (base–to–distance ratio ≈1:2.5).

In the network 2, control points were measured in various image pairs with base–to–distance ratio about 1:2. Minimal and maximal check point differences between reference and calculated coordinates are given in Table 1. Mean differences are given in Table2. RMS Errors are given in tTable 3. As mean differences are quite large compared to corresponding errors given in Table 3, check point differences must have been affected by systematic shift off all network. The relative accuracy should therefore be significantly better than the absolute accuracy. To estimate the relative accuracy, the RMSE was calculated after subtracting from differences their mean values. Relative accuracies are given in Table 4.

network	$v_X^{\min}$	$v_X^{\max}$	$v_Y^{\min}$	$v_Y^{\max}$	$v_Y^{\min}$	$v_Z^{\max}$
1a	-20	17	-28	-17	-11	-7
1b	-15	8	-35	-23	20	30
2	-8	4	4	10	-3	8

Table 1. Minimal and maximal check point differences [mm]

network	$v_X^{\min}$	v_Y^{mean}	v_Y^{mean}
1a	0	-24	-9
1b	-5	-26	24
2	-3	7	4

Table 2. Mean check point differences [mm]

network	$RMSE_X$	$RMSE_Y$	$RMSE_Z$
1a	10	24	9
1b	8	26	24
2	5	7	5

Table 3. Absolute accuracies [mm]

network	$RMSE_X$	$RMSE_Y$	$RMSE_Z$
1a	11	3	2
1b	7	3	3
2	4	2	2

Table 4. Relative accuracies [mm]

The RMSE of *Y* and *Z* coordinates calculated for networks 1a and 1b are about 0.5 of terrain pixel size. As the image axes were nearly parallel to *X* coordinate system axis, the $RMSE_X$ reached higher values (close to terrain pixel size).

5. DISCUSSION

In classical photogrammetric network, with ground control points, the image configuration is suited to the shape of modelled object and accuracy demands. The base–to–distance ratios and terrain pixel size must provide sufficient accuracy of determined point coordinates. Required accuracy of EO parameters of images or absolute orientation parameters of stereo models is usually satisfied by appropriate distribution of control points. However not all network configurations, that seem optimal in photogrammetry basing on indirect geo–referencing, should be preferred in bundle adjustment of directly geo–referenced images, especially when using low–cost MMS. For example the 1a network, which seems to be suited for modelling the building façade, may cause problems when solved without control points but with observed EO parameters instead. In this network the gross errors of observed PC coordinates of outermost images will cause errors of estimated EO parameters. Such errors may not be detected using standardized correction test. Besides, the *v* angles are estimated using mostly *v* observations, which errors (highly correlated with IMU *roll* errors) may be high when using the low–cost MEMS IMU.

When planning the network with directly geo–referenced images, using GPS and low–cost IMU, it is important to take into account not only the object characteristics and accuracy demands, but also the reliability of observed EO parameters. For example adding a second strip of images or projecting a closed looped network, will raise the controllability of potentially erroneous observations. Besides, modelling the object using outermost images should be avoided, as EO parameters of such images can be considerably affected by errors of observed EO parameters.

The accuracies obtained for the tested networks, show that the constructed MMS can be used for large scale, small area modelling. It seems to be appropriate for modelling of small buildings or architectural objects (like shrines), that give the opportunity to take images in the closed loop–configurations. However accuracies obtained for the building façade are also satisfactory.

6. REFERENCES

Bartelsen J., Mayer H., 2010. *Orientation of Image Sequences Acquired from UAVS and with GPS Cameras*, EuroCOW 2010, Castelldefels, Spain

Bayoud, F.A., 2006. *Development of a Robotic Mobile Mapping System by Vision-Aided Inertail Navigation: A Geomatics Approach*, Geodätisch-geophysikalische Arbeiten in der Schweiz, Schweizerischen Geodätischen Kommission

Coppa U., Guarnieri A., Pirotti F., Vettore A., 2007. *A Backpack MMS Application*, The 5th International Symposium on Mobile Mapping Technology, Padua, Italy

da Silva J. F., Camargo P., Gallis R. B. A., 2003. *Developement of a Low-cost Mobile Mapping System: A South American Experience*, Photogrammetric Record, 18(101), pp. 5-26

Ellum C.M., El-Sheimy N., 2001. *A Mobile Mapping System for the Survey Community*, Proceedings of the 3rd International Symposium on Mobile Mapping Technology Session 4, Cairo, Egypt

Haala N., Böhm J., 2003. *A Multi-sensor System for Positioning in Urban Environments*, ISPRS Journal of Photogrammetry & Remote Sensing 58(2003), pp. 31-42

Kolecki J., Kuras P., 2011. *Low-cost attitude and heading reference sensors in terrestrial photogrammetry – testing and calibration*, 7th International Symposium on Mobile Mapping Technology, Kraków, Poland

Kraus K., 1997. *Photogrammetry*. Vol. 2, Advanced Methods and Applications, Ferd. Duemmlers Verlag, Bonn

Luhmann T., Robson S., Kyle S., Harley I., 2006. *Close Range Photogrammetry*, Whittles Publishing, Dunbeath

Madeira S., Gonçalves J., Bastos L., 2008. *Low Cost Mobile Mapping System for Urban Surveys*, 13th FIG Symposium on Deformation Measurement and Analysis, pp 12-15, LNEC, Lisbon, Portugal

Piras M., Cina A., Lingua A., 2008. *Low Cost Mobile Mapping Systems: an Italian Experience*, PLANS 2008 Proceedings, Monterey, CA, USA

Wrobel B., Klemm D., 1984. *Ueber die Vermeidung singulaerer Faelle bei der Berechnung allgemeiner raeumlicher Drehungen*, International Archives of Photogrammetry and Remote Sensing 25, pp. 1153-1163, Rio de Janeiro, Brasil

Ellum, C.M., El-Sheimy, N., 2005. *Integrating Photogrammetry and GPS at the Measurement-Level*. Proceedings of ION GNSS 2005, Long Beach, CA, USA